

# Autonomous Exploitation of Reaction Pathways for Electrochemical C–N Coupling on Single-Atom Catalysts

Junjie Pan,<sup>#</sup> Haowen Ding,<sup>#</sup> Xinzhe Yang,<sup>#</sup> Xianhui Liang, Shanglin Wu, Mingzheng Zhang, Shunning Li,<sup>\*</sup> Shisheng Zheng,<sup>\*</sup> and Feng Pan<sup>\*</sup>



Cite This: *ACS Catal.* 2025, 15, 457–467



Read Online

ACCESS |

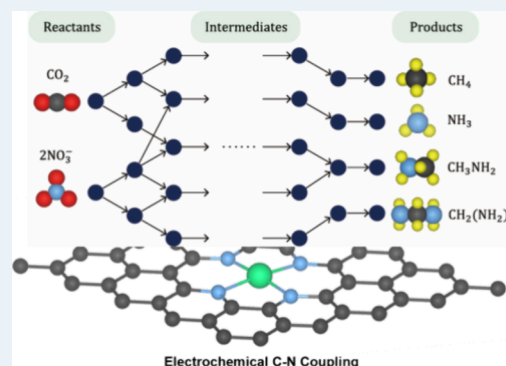
Metrics & More

Article Recommendations

Supporting Information

**ABSTRACT:** Electrochemical C–N coupling between CO<sub>2</sub> and N-containing small molecules is a promising strategy to close both the carbon and nitrogen loops to support the establishment of a net-zero carbon economy. However, the intricate reaction network and the contentious C–N coupling mechanism hinder the development of efficient electrocatalysts for industrial applications. Herein, we develop a graph-based approach to enable autonomous analysis of the C–N coupling mechanism for coreduction of CO<sub>2</sub> and NO<sub>3</sub><sup>−</sup> on single-atom catalysts (SACs). 1400 potential intermediates and 2490 C–N coupling modes are investigated based on the Cu–N<sub>4</sub>–C prototypical catalyst. We demonstrate that N-containing species with a higher reduction degree are more likely to undergo C–N coupling and the initial coupling of the C–N bond tends to occur on CO<sub>2</sub>. It is revealed that the hydrogenation energies of \*NH<sub>2</sub> and CO<sub>2</sub>, as well as their coupling energies, can serve as key indicators for catalyst recommendation. Using this approach, SACs with Mo, W, or Sb metal centers are identified as promising electrocatalysts for C–N coupling. This work presents a paradigm for automatically exploring the mechanisms of complex electrocatalytic reactions and offers a strategy for predicting highly active and selective SACs.

**KEYWORDS:** electrochemical C–N coupling, single-atom catalyst, graph theory, density functional theory, reaction network



## INTRODUCTION

The decarbonization of the chemical industry poses a significant challenge as we seek to reduce our dependence on fossil resources.<sup>1,2</sup> Electrochemical CO<sub>2</sub> reduction reactions (CO<sub>2</sub>RR) driven by renewable energy have emerged as a promising strategy for converting CO<sub>2</sub> into value-added products to achieve carbon neutrality or carbon negativity.<sup>3–5</sup> Despite the impressive progresses of electrocatalysts in generating a range of single-carbon (C<sub>1</sub>) and multicarbon (C<sub>2+</sub>) products containing C–H, C–C, and/or C–O bonds, their potential to produce higher value and diversified products is currently limited by the use of CO<sub>2</sub> and proton sources as the sole reactants.<sup>6</sup> Compared to the pure CO<sub>2</sub>RR, the combination of CO<sub>2</sub>RR with the electrochemical reduction of N-integrated small molecules (N<sub>2</sub>, NO, NO<sub>2</sub>, NO<sub>3</sub><sup>−</sup>, NH<sub>3</sub>, etc.) to generate C–N bond-containing compounds, e.g., urea and amine, presents a promising strategy for economical production of valuable organonitrogen products.<sup>7–19</sup> These compounds have widespread applications in chemical production, drug development, farming, and aerospace manufacturing, making this approach highly appealing.<sup>8</sup>

The diverse chemical bond properties of N-containing small molecules give rise to numerous potential reaction modes for C–N coupling, particularly when employing NO<sub>x</sub>, e.g., NO<sub>3</sub><sup>−</sup>, as the nitrogen sources. Residues of pesticides and fertilizers, as

well as industrial wastewater, carry significant amounts of NO<sub>3</sub><sup>−</sup> that can seep into groundwater and pose health risks to humans.<sup>20,21</sup> The reduction of NO<sub>3</sub><sup>−</sup> can effectively recycle it to prevent harm to the environment. Additionally, the dissociation energy of NO<sub>3</sub><sup>−</sup> (204 kJ mol<sup>−1</sup>) is relatively low in N-containing small molecules, especially when compared with the inert N<sub>2</sub> molecules (941 kJ mol<sup>−1</sup>).<sup>8</sup> NO<sub>3</sub><sup>−</sup> is reduced to ammonia (NH<sub>3</sub>) via an intricate eight-electron process,<sup>22</sup> with most of the intermediates presenting the possibility of coupling with the CO<sub>2</sub>-reduced intermediate to form a C–N bond. This complexity has left current research on the mechanism of C–N coupling in its early stages. Experimental techniques such as in situ Raman and infrared spectroscopy can be conducted to determine the types of chemical bonds present, but specifically identifying the intermediates involved in C–N coupling can often prove challenging.<sup>10,11</sup>

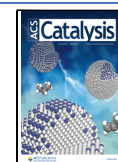
Density functional theory (DFT) simulations offer an efficient way to explore the underlying reaction mechanisms

**Received:** September 19, 2024

**Revised:** December 11, 2024

**Accepted:** December 12, 2024

**Published:** December 19, 2024



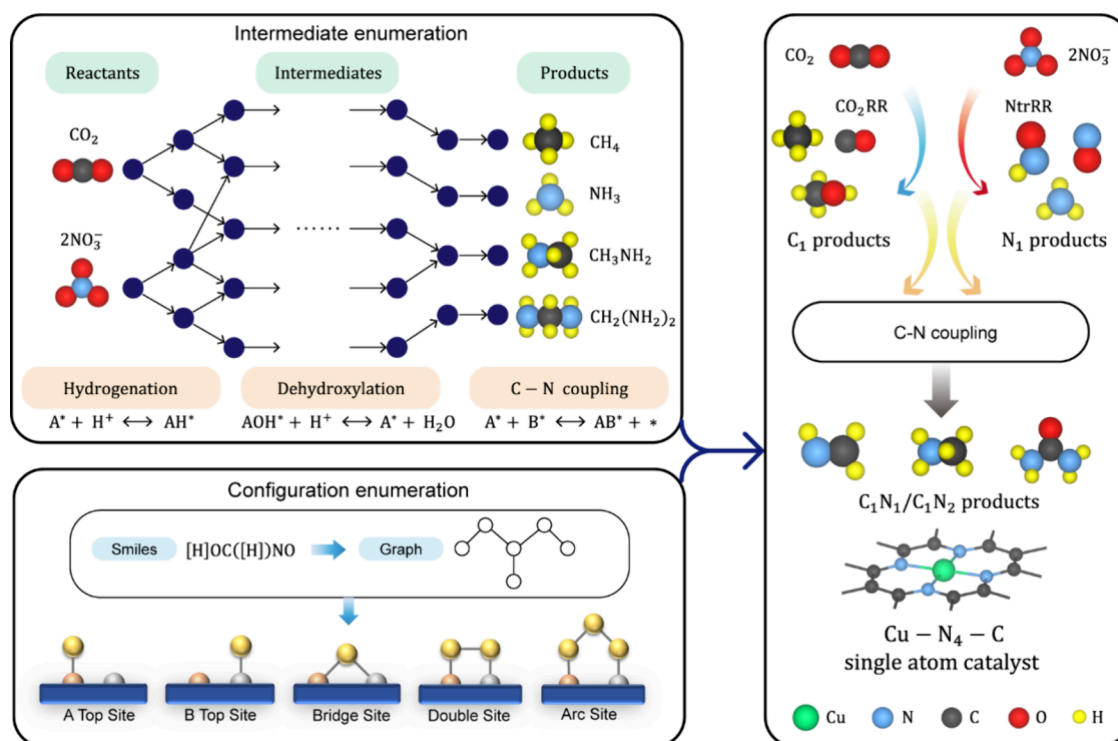


**Figure 1.** Flowchart of reaction network construction. The intermediates' enumeration and corresponding adsorption configuration enumeration are sequentially carried out.

for catalytic reactions.<sup>23–28</sup> This research paradigm typically involves a manual enumeration of the possible intermediates involved between the reactants and products to form an overall reaction network.<sup>29–31</sup> Subsequently, the possible adsorption configurations of these intermediates on the catalyst surface are enumerated and evaluated through DFT calculations to determine the preferred reaction pathways in terms of their thermodynamic and kinetic properties. This strategy has already been widely used to investigate the reaction mechanism for chemical processes that only involve a limited number of intermediates, such as oxygen evolution reaction (OER), CO<sub>2</sub> reduction reaction (CRR), nitrogen reduction reaction (NRR), and so on.<sup>32–36</sup> Although DFT calculations have been a success for these relatively simple reactions, they are impractical for more complex catalytic processes, such as the coreduction of CO<sub>2</sub> and NO<sub>3</sub><sup>−</sup> to form C–N bond-containing compounds, since the reaction network may include hundreds and thousands of intermediates. Notably, the challenge is not merely the complexity in the reaction network; extra complexity will arise due to the relatively large molecule size of the intermediates. Consequently, a variety of adsorption configurations can emerge for each intermediate on the catalyst surface.<sup>37,38</sup> The identification of the most stable adsorption configuration is critical in determining the preferred reaction pathway. The combinatorial size of these two hierarchical levels of complexity has forced researchers to make assumptions and eliminate some of the intermediates so that the computational burden could be reduced when investigating the reaction pathways. However, this approach will possibly overlook important reaction intermediates and elementary steps, resulting in misidentification of the preferred reaction pathway.<sup>30,39</sup> A detailed understanding of the reaction mechanism of C–N coupling is, therefore, difficult to achieve, which hinders the rational design of the related electrocatalysts.

Under this circumstance, developing a method that can generate and analyze the complex catalytic reaction network in an automated way is urgently needed for further advancing the field of electrochemical C–N coupling.

In this work, we develop a graph-based automatic approach for systematic analysis of the reaction pathways for the coreduction of CO<sub>2</sub> and N-containing small molecules to C–N bond-containing products. This approach enables the automation of reaction network generation and the enumeration of the adsorption configurations of intermediates. We employed the coreduction of NO<sub>3</sub><sup>−</sup> and CO<sub>2</sub> on a Cu–N<sub>4</sub>–C single-atom catalyst (SAC) as a demonstration platform for our algorithm.<sup>15</sup> SACs are at the forefront of catalytic research due to their high atom utilization efficiency, high catalytic activity, and low cost<sup>40–43</sup> and have recently been shown to be capable of achieving electrochemical C–N coupling.<sup>11,14,15,18</sup> It was found that the reaction network can contain up to more than 1400 possible intermediate species and 2490 possible C–N coupling modes. The energy required for C–N coupling is directly related to the degree of reduction for N-containing species, which can be attributed to the increased nucleophilicity of N species with a higher reduction degree. The initial coupling of the C–N bond tends to utilize gaseous CO<sub>2</sub> as the carbon source. Based on this critical finding, we propose that the hydrogenation energies of \*NH<sub>2</sub> and CO<sub>2</sub>, as well as their coupling energies, can serve as the key indicators for the rapid screening of potential electrocatalysts. Collectively, we have developed an algorithm for automatically analyzing the reaction networks, which enables high-throughput exploration of atomic-level mechanisms for complex electrocatalytic reactions and facilitates the rational design of related electrocatalysts.

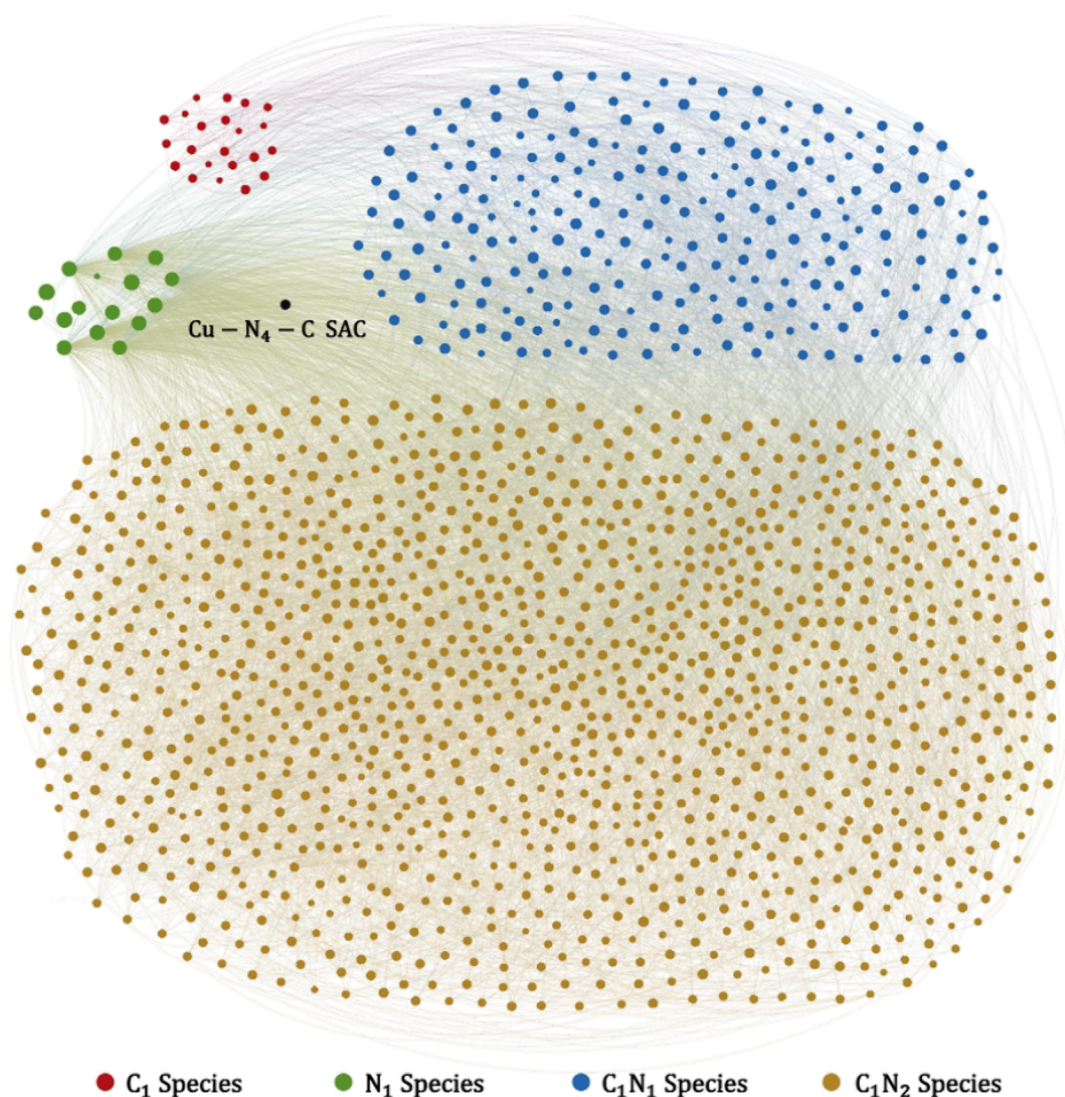


**Figure 2.** Reaction network for intermediates on the Cu–N<sub>4</sub>–C SAC. Red dots represent C<sub>1</sub> intermediates, green dots represent N<sub>1</sub> intermediates, blue dots represent C<sub>1</sub>N<sub>1</sub> intermediates, and orange dots represent C<sub>1</sub>N<sub>2</sub> intermediates. The size of nodes is positively correlated with the size of degrees.

## RESULTS AND DISCUSSION

The electrochemical coreduction of CO<sub>2</sub> and NO<sub>3</sub><sup>−</sup> to synthesize compounds containing one carbon and two nitrogen atoms, such as urea, has gained considerable attention recently. Here, we showcase the capability of our algorithm by analyzing a reaction network involving one CO<sub>2</sub> and two NO<sub>3</sub><sup>−</sup> molecules as reactants and CH<sub>2</sub>(NH<sub>2</sub>)<sub>2</sub> as the ending product (Figure 1). The CH<sub>2</sub>(NH<sub>2</sub>)<sub>2</sub> is chosen as the end point of the reaction network because it represents the fully hydrogenated state of both C and N, making it the most reduced product from the coreduction of CO<sub>2</sub> and two NO<sub>3</sub><sup>−</sup>.

The initial stage is to enumerate all the possible intermediates connecting the reactants and the products to build the pool of potential intermediates, which is achieved by a molecule graph-based enumeration algorithm with RDKit.<sup>44</sup> In a molecule graph, atoms are represented as nodes and chemical bonds are abstracted as edges connecting these nodes.<sup>45,46</sup> The graph-based representation of molecules is convenient for computer recognition and manipulation because the graph can be further transformed into a matrix or SMILES representation. Considering that the reactants of

CO<sub>2</sub> and NO<sub>3</sub><sup>−</sup> are converted to be as molecule graphs, the generation of intermediates can be iteratively implemented by editing the graph with preset elementary step types, such as hydrogenation and C–N coupling. In this process, the boundary conditions are applied to check whether the generated intermediate violates the bonding principles. Specifically, the number of chemical bonds that N atoms, C atoms, and O atoms can form is limited to 4, 4, and 2, respectively. Those valid intermediates will be added into the pool with their corresponding elementary steps, and the algorithm continues to generate new intermediates until CH<sub>2</sub>(NH<sub>2</sub>)<sub>2</sub> is included (more details are shown in Figure S1). Once all possible intermediate species are obtained, the next step is to construct the adsorption structures of each intermediate on the surface. This requires the definition of the possible active sites on the catalytic surface. Previous works have demonstrated that in M–N–C single-atom catalysts, not only the metal center but also the surrounding coordination atoms may exhibit catalytic activity.<sup>47,48</sup> Thus, we considered Cu and N as the possible active sites and defined five possible adsorption modes, namely, the Cu top site, N top site, Cu–N

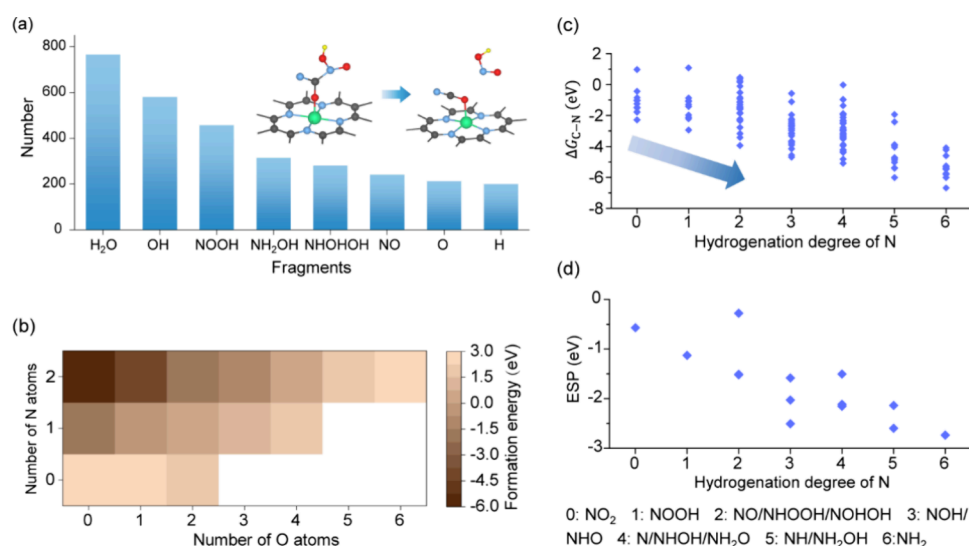


**Figure 3.** (a) Number of decomposition fragments from the decomposed configurations. The inset shows the initial configuration and optimized configuration of a typical structure (CONNOOH) with the NOOH group detaching. (b) Relationship between the formation energy and the number of N and O atoms. A blank grid indicates that the corresponding configuration does not exist. (c) Relationship between the free energy of the coupling reaction between  $C_1$  and  $N_1$  and the degree of hydrogenation of  $N_1$  intermediates. (d) Relationship between the electrostatic potential and the degree of hydrogenation of  $N_1$  species. Note that the NOHOH and NHOOH overlap in the figure.

bridge site, Cu–N double, and Cu–N Arc (lower panel of Figure 1). Subsequently, we enumerated possible surface-binding atom or atoms of each intermediate considering these five adsorption modes. The geometric rules and the connectivity of molecular graph are then applied to generate different adsorption configurations for DFT calculation (more details are provided in the Methods Section).

The overall resultant reaction network includes a total of 1478 intermediates and more than 8168 elementary steps (Figure 2). The intermediates are clustered into four categories according to the number of carbon and nitrogen atoms. The amounts of  $C_1$  intermediates,  $N_1$  intermediates,  $C_1N_1$  intermediates, and  $C_1N_2$  intermediates are 22, 16, 240, and 1200, respectively. For the elementary steps, there are a total of 3914 hydrogenation reactions, 1764 dehydroxylation reactions, and 2490 C–N coupling reactions. The reaction network can also be treated as a graph, in which the node is the intermediate and the edge is the elementary step.<sup>49,50</sup> By employing the simple path algorithm<sup>51</sup> in the graph theory, we can obtain the number of reaction pathway for each possible product starting from the reactants (Table S1). For example, there exist 14 distinct pathways from CO<sub>2</sub> to CH<sub>4</sub>. Urea (CO(NH<sub>2</sub>)<sub>2</sub>), a typical product for electrochemical C–N coupling, has 130,332 different reaction pathways from the reactants with at least one intermediate different. It turns out that this task is beyond our capability upon manual exploration. In graph theory, the degree of a node represents the number of edges connected to this node, which indicates the number of potential reactions that a specific intermediate involves. The  $N_1$  intermediates exhibit the highest average degree among all of the intermediates (Table S2), as they are capable of participating in both hydrogenation reactions and C–N coupling reactions with  $C_1$  or  $C_1N_1$  intermediates. The number of degrees in  $C_1N_1$  and  $C_1N_2$  intermediates positively correlates with their average number of adsorption configurations on the surface because the species with higher degrees generally contain more unsaturated atoms and thus more adsorption modes (Figure S2).

After obtaining the intermediates and their corresponding adsorption configurations, we conducted a high-throughput DFT calculation procedure. To reduce the computational cost, we assessed the stability of each adsorption structure during the optimization process (details provided in the Methods Section). If a structure is found to undergo decomposition or reconstruction, the optimization calculation will be stopped since a stable structure is a prerequisite for a specific reaction to occur. The configuration of the DFT-calculated structures is converted to a graph by determining the connectivity between atoms. The graph isomorphism algorithm is then employed to compare whether there are any connectivity changes in the molecule graph. The stable structures are continually optimized until the force convergence.

According to the calculation results (Table S3), 3586 adsorption configurations will suffer structure decomposition or reconstruction, resulting in 665 intermediates that cannot form any stable configurations at the catalyst surface. The unstable intermediates may stem from the intrinsic properties of the intermediates and the interaction between the intermediates and the catalytic surface. The molecule fragments generated by the decomposed and reconstructed configurations are sorted by frequency of occurrence (Figure 3a). The incidence of H<sub>2</sub>O fragments is the most frequent. The larger the number of atoms the configuration accommodates, the higher the likelihood of its decomposition to generate H<sub>2</sub>O (Figure S3). This is because intermediates with more atoms tend to contain more O–H bonds, while H<sub>2</sub>O is a relatively stable molecule, making intramolecular dehydration more likely to occur. When the H<sub>2</sub>O molecule is not formed, the hydroxyl groups and oxygen also have a tendency to detach (Figure 3a). Consequently, the products that contain a significant amount of oxygen or hydroxyl groups may not easily form in electrochemical C–N coupling. Following the fact that the H<sub>2</sub>O and hydroxyl fragments are the N-containing fragments, including NOOH, NH<sub>2</sub>OH, NHOHOH, and NO, due to the presence of lone pair electrons or the formation of large  $\pi$  bonds, these N-containing intermediates can exist

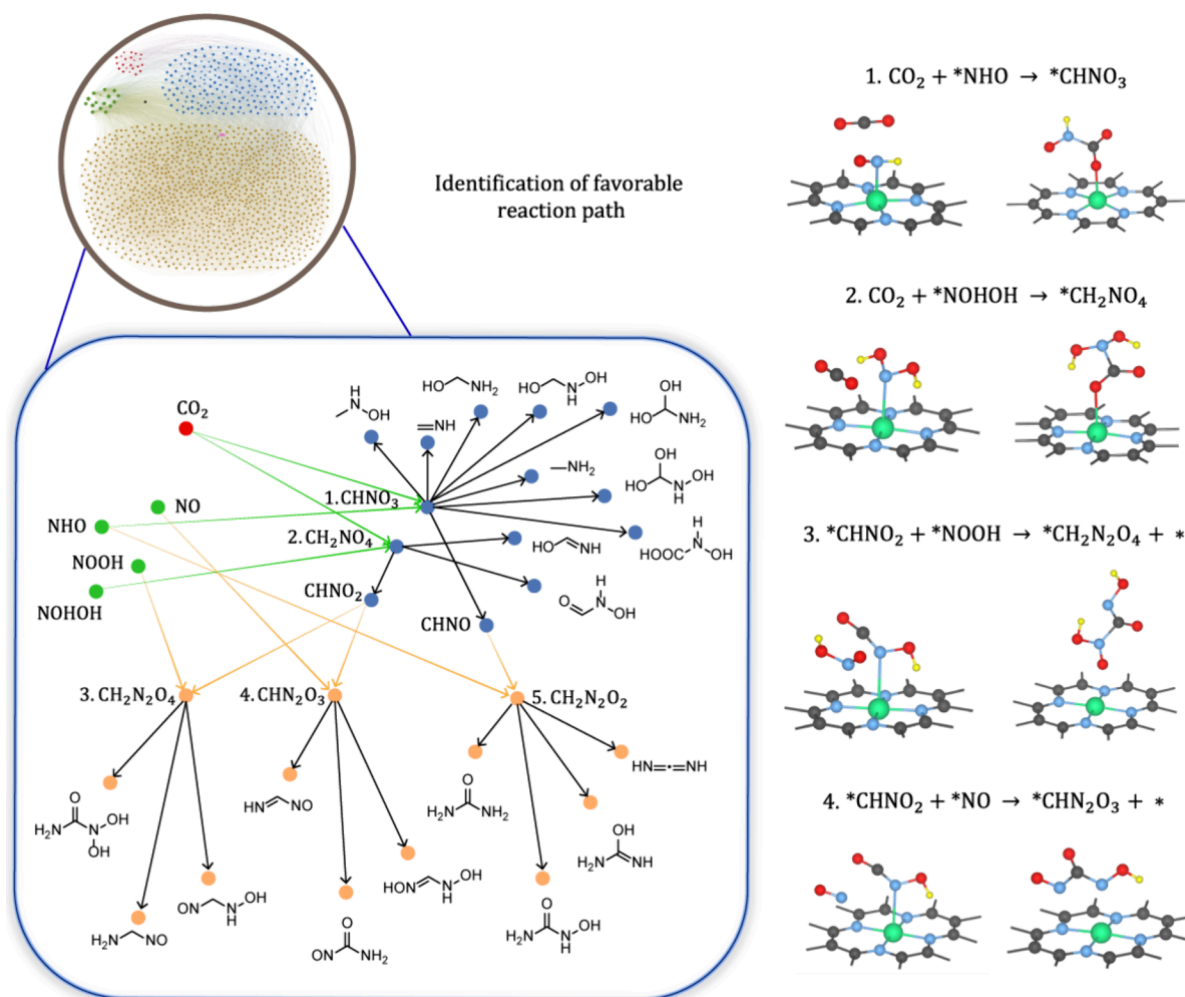


**Figure 4.** C–N coupling steps correspond to different possible products. Green lines represent the coupling between  $\text{C}_1$  and  $\text{N}_1$  intermediates, and orange lines represent the coupling between  $\text{C}_1\text{N}_1$  and  $\text{N}_1$  intermediates. The right panel shows the initial and final configurations of the most frequent C–N coupling modes in the formation pathways of these products.

independently and remain stable (Figure S4). However, this also makes it difficult for them to form a C–N bond with C-containing intermediates.

For the 813 stable intermediates, we analyzed their lowest energy configurations. Among them, 290 intermediates tend to be physically adsorbed near the interface (Figure S4), indicating a greater likelihood of desorption to become products or migration at the interface for C–N coupling with other species. In the case of 523 species chemisorbed on the interface, we conducted an analysis of the atoms involved in their interactions. While most of them tend to adsorb on the Cu metal center, a significant proportion of structures exhibit a preference for adsorption on the surrounding N/C atoms (Figures S5 and S6). This indicates that N/C atoms can also act as active centers, which creates favorable conditions for the occurrence of C–N coupling since the C–N coupling requires a local enrichment of intermediates. Simultaneously, this suggests that by modifying the types of nonmetal atoms coordinated to the metal center, researchers may fine-tune the performance of electrochemical C–N coupling. This strategy has already been demonstrated to be effective in reactions such as ORR.<sup>48</sup>

Then, we calculated the formation energies of these lowest energy configurations (Figure 3b). Intermediates containing

more O atoms tend to have higher average formation energies, whereas those containing more N atoms tend to have lower average formation energy. The  $\text{C}_1\text{N}_2$  intermediates have the lowest formation energy, indicating that the coreduction of  $\text{CO}_2$  and  $\text{NO}_3^-$  becomes easier as more hydrogenation steps are carried out. The rate-determining step of the reaction is more likely to occur during the hydrogenation of  $\text{C}_1/\text{N}_1$  species or the C–N coupling of  $\text{C}_1$  and  $\text{N}_1$  intermediates. We calculated the reaction energies of all possible  $\text{C}_1$ – $\text{N}_1$  coupling steps. Theoretically, there could be 300  $\text{C}_1$ – $\text{N}_1$  coupling modes since there are 20 intermediates solely from  $\text{CO}_2$  reduction and 15 intermediates solely from  $\text{NO}_3^-$  reduction. However, there are indeed only 110  $\text{C}_1$ – $\text{N}_1$  coupling steps due to the electronic structure of some intermediates being saturated, and some intermediates after C–N coupling become unstable at the interface. The results (Figure 3c) show that the higher the degree of hydrogenation the N-containing species undergo, the smaller the energy consumption will be in  $\text{C}_1$ – $\text{N}_1$  coupling. This trend is correlated to the change in electrostatic potential of  $\text{N}_1$  intermediates (Figure 3d), which is negatively correlated with the degree of hydrogenation. The lower the electrostatic potential of the intermediates, the stronger the nucleophilicity and the more easily they can attack the carbon atom, which explains why the  $\text{N}_1$  intermediates with a high degree of

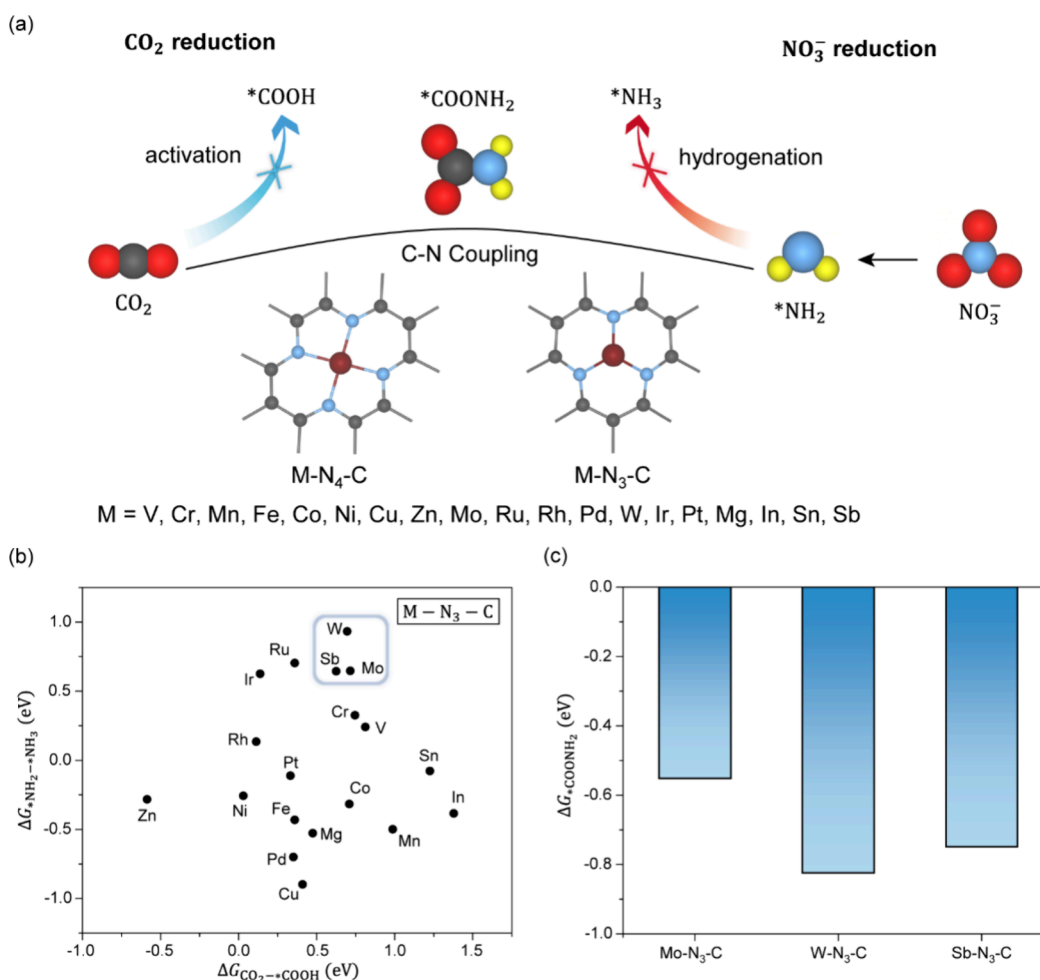


**Figure 5.** (a) Schematic diagram of CO<sub>2</sub> and \*NH<sub>2</sub> coupling on M-N<sub>4</sub>-C and M-N<sub>3</sub>-C to generate \*COONH<sub>2</sub>. (b) Free energy of the CO<sub>2</sub> activation and \*NH<sub>2</sub> hydrogenation steps on M-N<sub>3</sub>-C. (c) Free energy of CO<sub>2</sub> and \*NH<sub>2</sub> coupling on Mo-N<sub>3</sub>-C, W-N<sub>3</sub>-C, and Sb-N<sub>3</sub>-C.

hydrogenation are more likely to participate in the C–N coupling reaction. It is worth noting that the trend in electrostatic potential change is independent of the catalytic surface. Hence, we speculate that this pattern may hold true for other catalysts as well, as supported by recent studies demonstrating that the coupling between carbon-containing species and \*NH<sub>2</sub> is generally energetically exothermic.<sup>15,16,52–54</sup>

We select 35 possible products from the coreduction of CO<sub>2</sub> and NO<sub>3</sub><sup>−</sup> (Table S1) to analyze the C–N coupling mode when generating a particular product. The results show that the initial C–N coupling step for all products generally involves the combination of CO<sub>2</sub> and nitrogen-containing species, e.g., NOHOH and NHO (Figure 4 and Table S4). This is because the activation of CO<sub>2</sub> to form \*COOH requires a relatively high energy input on Cu–N<sub>4</sub>-C (1.60 eV, Figure S7). According to the Arrhenius equation and approximating this process as a first-order reaction, it can be inferred that CO<sub>2</sub> can exist at the interface for a long time, which also helps reduce the formation of byproduct CO. On the other hand, the energy needed for the coupling of CO<sub>2</sub> and nitrogen-containing species is comparatively low (Table S5). The formation of the second C–N bond in the C<sub>1</sub>N<sub>2</sub> products also shows a preference toward nitrogen-containing species that have undergone a certain degree of hydrogenation (NOHOH/NHO) (Figure 4, details provided in Table S4), which further

supports the pattern observed in Figure 3c. Notably, we found that when participating in the C–N coupling process, CO<sub>2</sub> tends to remain in a physisorbed state near the active sites, while nitrogen-containing species approach and bond with Cu single atoms at the interface. Therefore, we did not consider the \*CO<sub>2</sub><sup>−</sup> chemisorbed state of CO<sub>2</sub>.

Although various products can be generated, CO(NH<sub>2</sub>)<sub>2</sub> is found to be the major C–N bond-containing product in the experiments.<sup>8,55</sup> In general, intermediates with fewer oxygen atoms and more nitrogen atoms tend to have lower formation energies. CO(NH<sub>2</sub>)<sub>2</sub>, which contains only one oxygen atom and two deeply reduced \*NH<sub>2</sub> groups, is thus thermodynamically favored (Figures S8 and S9). It is worth noting that the energy required for further hydrogenation of CON<sub>2</sub>H<sub>4</sub> to COHN<sub>2</sub>H<sub>4</sub> increases sharply ( $\Delta G = 1.54$  eV, Figure S10), which limits the possibility of its further reduction and makes it more likely to desorb as the final product ( $\Delta G_{\text{desorb}} = 0.34$  eV). However, on Cu–N<sub>4</sub>-C, the pathway for the reduction of NO<sub>3</sub><sup>−</sup> to NH<sub>3</sub> is also energetically favorable (Figure S11). The free energy of the rate-determining step is only 0.42 eV, which results in the formation of a significant amount of byproduct NH<sub>3</sub>.<sup>15</sup>

From the above analysis, it can be concluded that an effective electrocatalyst for CO<sub>2</sub> and NO<sub>3</sub><sup>−</sup> coreduction could have appropriate resistance for CO<sub>2</sub> hydrogenation, which can facilitate the direct coupling of CO<sub>2</sub> and nitrogen-containing

species while reducing the generation of carbon-containing byproducts such as CO (Figure 5a). Concurrently, for the reduction of  $\text{NO}_3^-$ , it is ideal to have an intermediate species with a highly hydrogenated state that can remain stable at the interface for an extended period. This will enable the coupling of  $\text{CO}_2$  and the intermediate species to form C–N bonds.  $^*\text{NH}_2$  represents an optimal candidate for this role, as the reaction energy for the coupling between  $^*\text{NH}_2$  and  $\text{CO}_2$  is the lowest. From the perspective of the electronic structure,  $^*\text{NH}_2$  is also likely to be stabilized on the active center. There still be an  $\text{sp}^3$  hybrid orbital of the N atom in  $^*\text{NH}_2$  half-filled. On the contrary, all four  $\text{sp}^3$  hybrid orbitals are fully filled in  $\text{NH}_3$ , resulting in a less stable adsorption of  $\text{NH}_3$  on the metal center compared to  $^*\text{NH}_2$ . Consequently, the free energy change for  $^*\text{NH}_2 + \text{H}^+ + e^- = ^*\text{NH}_3$  has a tendency to be uphill in essence.<sup>56,57</sup>

Based on the above knowledge, we calculated the free energy changes of the  $\text{CO}_2$  activation and  $^*\text{NH}_2$  hydrogenation steps on 38 single-atom catalysts with M- $\text{N}_4$ -C and M- $\text{N}_3$ -C structures (M = V, Cr, Mn, Fe, Co, Ni, Cu, Zn, Mo, Ru, Rh, Pd, W, Ir, Pt, Mg, In, Sn, and Sb, Figure 5a), all of which can be experimentally synthesized.<sup>58–61</sup> The results show that for the M- $\text{N}_4$ -C structure,  $\Delta G(\text{CO}_2 \rightarrow ^*\text{COOH})$  and  $\Delta G(^*\text{NH}_2 \rightarrow ^*\text{NH}_3)$  are negatively correlated, indicating that the M- $\text{N}_4$ -C SAC may not be efficient for C–N bond formation with high selectivity (Figure S12). The Faradaic efficiency of the recently reported Cu- $\text{N}_4$ -C and Co- $\text{N}_4$ -C with the reactants of  $\text{NO}_3^-$  and  $\text{CO}_2$  to generate products containing C–N bonds is indeed not higher than 30%.<sup>11,15</sup> The Mo- $\text{N}_3$ -C, W- $\text{N}_3$ -C, and Sb- $\text{N}_3$ -C can satisfy both requirements with the corresponding free energy change exceeding 0.5 eV (Figure 5b). The reaction energies for the  $\text{CO}_2$  and  $^*\text{NH}_2$  coupling are also low on these catalysts (Figure 5c). Moreover, we calculated the complete pathway of  $\text{NO}_3^-$  reduction to  $^*\text{NH}_2$  on these three catalysts, and the results show that the formation of  $^*\text{NH}_2$  is favorable (Figures S13–S15). These suggest that the Mo- $\text{N}_3$ -C, W- $\text{N}_3$ -C, and Sb- $\text{N}_3$ -C are capable of efficient C–N coupling and thus are likely to be excellent  $\text{CO}_2$  and  $\text{NO}_3^-$  coreduction catalysts.

As final remarks, we discuss the improvement directions in the future. The main goal of the proposed graph-based scheme is to enable pathway prediction, overpotential estimation, and the assessment of general trends across the reaction network, which can provide experimentally relevant insights into electrocatalysis. We acknowledge that this approach does not yet allow for selectivity predictions for specific products as this would require activation energy calculations and a microkinetic model. Performing kinetic calculations for systems with thousands of intermediates by DFT remains challenging. Machine learning potentials and pretrained models may offer a possible solution.<sup>62–64</sup> The solvent effects may influence the optimal reaction pathways toward the targeted products by the stabilizing effect of hydrogen bonding and the electrostatic interactions from cations, which are still difficult to consider in a high-throughput framework due to their complexity and variability.<sup>26,65–67</sup> A feasible solution is to perform empirical numerical corrections for intermediates with electron-withdrawing tendency.<sup>68</sup> Future models will also attempt to make performance predictions under constant potential conditions.<sup>69</sup>

## CONCLUSIONS

In summary, we have developed a graph-based high-throughput reaction network analysis algorithm, which can achieve automated enumeration of intermediates and corre-

sponding adsorption configurations. We have applied this framework to analyze the reaction mechanism of the coreduction of  $\text{NO}_3^-$  and  $\text{CO}_2$  on the Cu- $\text{N}_4$ -C SAC. It is revealed that  $\text{CO}_2$  can directly couple with N-containing species without the hydrogenation and that the higher the hydrogenation degree of N-containing species, the lower the reaction energy for C–N coupling. Based on the above knowledge, the Mo- $\text{N}_3$ -C, W- $\text{N}_3$ -C, and Sb- $\text{N}_3$ -C SACs are predicted to be efficient catalysts for C–N coupling. Our work provides a paradigm for the mechanism exploration of complex electrocatalytic reactions and the strategy to predict the related electrocatalysts.

## METHODS

**DFT calculations:** The spin-polarized DFT calculations were performed using the Vienna ab initio simulation package (VASP),<sup>70–72</sup> with the Perdew–Burke–Ernzerhof (PBE) exchange–correlation functional.<sup>73</sup> The projector augmented wave method (PAW)<sup>74,75</sup> with a plane-wave kinetic energy cutoff of 400 eV was used, and a k-mesh of  $2 \times 2 \times 1$  was adopted to sample the Brillouin zone. In structural relaxation, the total energy and the force on each relaxed atom were converged to  $10^{-5}$  eV and 0.05 eV  $\text{\AA}^{-1}$ , respectively. We first performed a 90-step ionic relaxation for each configuration. If the configuration was neither decomposed nor reconstructed and was determined to be stable based on the graph connectivity algorithm, it was further optimized until force convergence. The structure of Cu- $\text{N}_4$ -C was based on a one-layer two-dimensional graphene structure with a  $4 \times 4$  super cell lateral size. A vacuum layer of 20  $\text{\AA}$  in the z-direction was set to avoid unwanted interactions between periodic images. A VASPsol implicit solvation model was used for solvation corrections in our energy calculations.<sup>76</sup> A Debye screening length of 3  $\text{\AA}$  was chosen, as this corresponds to a bulk ion concentration of 1 M. The nonelectrostatic parameter TAU was set to zero to avoid numerical instabilities. For the C–N coupling steps involved in the 35 selected products, we performed barrier calculations using the CI-NEB method. Three images were inserted along the CI-NEB pathway, with a force tolerance set to 0.05 eV  $\text{\AA}^{-1}$ .

The calculated relative Gibbs free energy ( $\Delta G$ ) was evaluated as follows:

$$\Delta G = \Delta E + \Delta ZPE - T\Delta S + k_{\text{B}}T \ln(10) \times \text{pH} + eU \quad (1)$$

where  $\Delta E$  is the DFT-calculated relative energy,  $\Delta ZPE$  is the change in zero-point energy (ZPE), and  $\Delta S$  is the change in entropy. The ZPE and entropic contributions were calculated from the vibrational frequencies, which were obtained using the finite displacement method with only the degrees of freedom of adsorbates and the transition-metal single atom included. The last term corresponds to the free energy correction of pH. In this work, the free energy profiles were calculated at 0 V vs RHE and pH = 6.8.

The formation energies of each intermediate is calculated by

$$G_{\text{f}} = G_{\text{slab+ads}} - G_{\text{slab}} - \sum_{i \in \{\text{C,H,O,N}\}} n_i \mu_i \quad (2)$$

where  $G_{\text{slab+ads}}$  is the Gibbs free energy of the surface and adsorbate,  $G_{\text{slab}}$  is the Gibbs free energy of the surface slab,  $n_i$  is the number of atoms of species  $i$  in the adsorbate, and  $\mu_i$  are

the reference energies. In this case the reference energies are computed by<sup>30</sup>

$$\begin{aligned}\mu_{\text{H}} &= G_{\text{H}_2}/2 \\ \mu_{\text{O}} &= G_{\text{H}_2\text{O}} - G_{\text{H}_2} \\ \mu_{\text{C}} &= G_{\text{CO}_2} - 2\mu_{\text{O}} \\ \mu_{\text{N}} &= G_{\text{NO}_2} - 2\mu_{\text{O}}\end{aligned}\quad (3)$$

where  $G_j$  is the Gibbs free energy of species  $j$ .

$\Delta G_{\text{C-N}}$  represented in Figure 3c is calculated by

$$\Delta G_{\text{C-N}} = G_{\text{product}} - G_{\text{reactant}} - G_{\text{N}} \quad (4)$$

where  $G_{\text{product}}$  is the Gibbs free energy of products of the C–N coupling reaction,  $G_{\text{reactant}}$  is the Gibbs free energy of reactants of the C–N coupling reaction, including  $\text{C}_1$ ,  $\text{C}_1\text{N}_1$  species, and  $G_{\text{N}}$  is the formation energy of  $\text{N}_1$  species. For example,  $\Delta G_{\text{C-N}}(*\text{COONH}_2) = G_{*\text{COONH}_2} - G_{*\text{CO}_2} - G_{\text{NHO}}$ , and  $G_{\text{NHO}} = \mu_{\text{N}} + \mu_{\text{H}} + \mu_{\text{O}}$ .

The generation of species and adsorption configurations by graph theory: Because of the saturated electron configuration and steric hindrance of  $\text{NO}_3^-$ , it can hardly be an intermediate for C–N coupling. Thus, we used  $*\text{NO}_2$ , which is the direct reduction intermediate of  $\text{NO}_3^-$ , and  $\text{CO}_2$  as the reactants to generate the possible intermediates.

The RDKit,<sup>77</sup> which is an open-source tool for cheminformatics, is used to generate the possible species. The overall scheme is presented in Figure S1. To enumerate all species, we defined three types of elementary steps as follows:

1. Hydrogenation reaction, denoted as  $\text{A}^* + \text{H}^+ \leftrightarrow \text{AH}^*$ .
2. Dehydroxylation reaction, denoted as  $\text{AOH}^* + \text{H}^+ \leftrightarrow \text{A}^* + \text{H}_2\text{O}$ .
3. C–N coupling reaction, denoted as  $\text{A}^* + \text{B}^* \leftrightarrow \text{AB}^* + *$ .

The elementary step is realized by editing the molecular graphs with RDKit. Take the hydrogenation reaction as an example, the molecular graph of A will add a H node and an A–H edge and then become a new molecular graph of AH.

Meanwhile, the new species will be verified under several boundary conditions:

1. No more than four, four, and two bonds can be found on carbon, nitrogen, and oxygen atoms, respectively.
2. No more than two nitrogen atoms in each species.
3. No N–N bonds, N–O–N bonds, and N–O–C bonds. Notably, we also did not consider C–C coupling products as they were not experimentally observed on Cu–N–C.<sup>15</sup>

Subsequently, we considered the bond principles to ensure a bond reasonable of adatoms: the C atom and N atom can connect with up to three atoms, and the O atom can connect with up to one atom.

The geometric rules and the connectivity of the molecular graph are then applied to generate different adsorption configurations for DFT calculation. We defined five possible adsorption modes, namely, the Cu top site, N top site, Cu–N bridge site, Cu–N double, and Cu–N Arc site. The geometric rules are listed as follows:

1. For the Cu/N top site, the adatom was placed on the top site of one Cu/N active site, and the distance is set to the sum of the radii of the adatoms and Cu/N atoms.

2. For the Cu–N bridge site, the adatom was placed on the plane that passes through the bridge site of Cu and N active sites. The distances between the adatom and the two atoms are equivalent to corresponding radii summation  $d$ .
3. For the Cu–N double site, two adatoms were initially placed vertically above on the Cu and N active sites. Then, they move on the plane that passes through these four atoms until the distance between them is equal to the sum of their radii. Note that the order of the two adatoms can be reversed.
4. For the Cu–N Arc site, two adatoms were initially placed vertically above on the Cu and N active sites according to their sum of atomic radii. Then, they moved away each other to ensure that the angle between the two adatoms and the interval atom would not be too small. The interval atom was placed via the same approach for the bridge site adsorption.

## ■ ASSOCIATED CONTENT

### Data Availability Statement

All data are available in the main manuscript or the Supporting Information. The related codes are positioned in <https://github.com/Jackistudy/graph-theory-code>.

### Supporting Information

The Supporting Information is available free of charge at <https://pubs.acs.org/doi/10.1021/acscatal.4c05751>.

Schematic diagram of possible products; reaction pathways of possible products; energy statistics for C–N coupling steps; atomic structure of intermediates; free energy diagram of reaction pathways (PDF)

## ■ AUTHOR INFORMATION

### Corresponding Authors

**Shunning Li** – School of Advanced Materials, Peking University, Shenzhen Graduate School, Shenzhen 518000, China; [orcid.org/0000-0002-5381-6025](https://orcid.org/0000-0002-5381-6025); Email: [lisin@pku.edu.cn](mailto:lisin@pku.edu.cn)

**Shisheng Zheng** – College of Energy, Xiamen University, Xiamen 361000, China; [orcid.org/0009-0000-4529-7440](https://orcid.org/0009-0000-4529-7440); Email: [zhengss@xmu.edu.cn](mailto:zhengss@xmu.edu.cn)

**Feng Pan** – School of Advanced Materials, Peking University, Shenzhen Graduate School, Shenzhen 518000, China; [orcid.org/0000-0002-8216-1339](https://orcid.org/0000-0002-8216-1339); Email: [panfeng@pku.edu.cn](mailto:panfeng@pku.edu.cn)

### Authors

**Junjie Pan** – School of Advanced Materials, Peking University, Shenzhen Graduate School, Shenzhen 518000, China

**Haowen Ding** – School of Advanced Materials, Peking University, Shenzhen Graduate School, Shenzhen 518000, China

**Xinzhe Yang** – School of Advanced Materials, Peking University, Shenzhen Graduate School, Shenzhen 518000, China; [orcid.org/0009-0008-1921-0629](https://orcid.org/0009-0008-1921-0629)

**Xianhui Liang** – College of Energy, Xiamen University, Xiamen 361000, China

**Shanglin Wu** – School of Advanced Materials, Peking University, Shenzhen Graduate School, Shenzhen 518000, China

Mingzheng Zhang — School of Advanced Materials, Peking University, Shenzhen Graduate School, Shenzhen 518000, China

Complete contact information is available at:  
<https://pubs.acs.org/10.1021/acscatal.4c05751>

### Author Contributions

<sup>#</sup>J.P., H.D., and X.Y. contributed equally.

### Notes

The authors declare no competing financial interest.

## ACKNOWLEDGMENTS

This work was supported by the National Natural Science Foundation of China (22402163, 22109003), Natural Science Foundation of Xiamen, China (3502Z202472001), the Soft Science Research Project of Guangdong Province (no. 2017B030301013), the Basic and Applied Basic Research Foundation of Guangdong Province (2021B1515130002), Shenzhen Key Laboratory of New Energy Resources Genome Preparation and Testing (no. ZDSYS201707281026184), and the Major Science and Technology Infrastructure Project of Material Genome Big-Science Facilities Platform supported by Municipal Development and Reform Commission of Shenzhen.

## REFERENCES

- (1) Ma, W.; He, X.; Wang, W.; Xie, S.; Zhang, Q.; Wang, Y. Electrocatalytic reduction of CO<sub>2</sub> and CO to multi-carbon compounds over Cu-based catalysts. *Chem. Soc. Rev.* **2021**, *50* (23), 12897–12914.
- (2) Wu, J.; Huang, Y.; Ye, W.; Li, Y. CO<sub>2</sub> reduction: from the electrochemical to photochemical approach. *Adv. Sci.* **2017**, *4* (11), 1700194.
- (3) Zhang, W.; Hu, Y.; Ma, L.; Zhu, G.; Wang, Y.; Xue, X.; Chen, R.; Yang, S.; Jin, Z. Progress and perspective of electrocatalytic CO<sub>2</sub> reduction for renewable carbonaceous fuels and chemicals. *Adv. Sci.* **2018**, *5* (1), 1700275.
- (4) Xie, H.; Wang, T.; Liang, J.; Li, Q.; Sun, S. Cu-based nanocatalysts for electrochemical reduction of CO<sub>2</sub>. *Nano Today* **2018**, *21*, 41–54.
- (5) Zhu, P.; Wang, H. High-purity and high-concentration liquid fuels through CO<sub>2</sub> electroreduction. *Nat. Catal.* **2021**, *4* (11), 943–951.
- (6) Tao, Z.; Rooney, C. L.; Liang, Y.; Wang, H. Accessing Organonitrogen Compounds via C-N Coupling in Electrocatalytic CO<sub>2</sub> Reduction. *J. Am. Chem. Soc.* **2021**, *143* (47), 19630–19642.
- (7) Li, J.; Zhang, Y.; Kuruvinschetti, K.; Kornienko, N. Construction of C-N bonds from small-molecule precursors through heterogeneous electrocatalysis. *Nat. Rev. Chem.* **2022**, *6* (5), 303–319.
- (8) Peng, X.; Zeng, L.; Wang, D.; Liu, Z.; Li, Y.; Li, Z.; Yang, B.; Lei, L.; Dai, L.; Hou, Y. Electrochemical C-N coupling of CO<sub>2</sub> and nitrogenous small molecules for the electrosynthesis of organonitrogen compounds. *Chem. Soc. Rev.* **2023**, *52* (6), 2193–2237.
- (9) Jouny, M.; Lv, J. J.; Cheng, T.; Ko, B. H.; Zhu, J. J.; Goddard, W. A., 3rd; Jiao, F. Formation of carbon-nitrogen bonds in carbon monoxide electrolysis. *Nat. Chem.* **2019**, *11* (9), 846–851.
- (10) Lv, C.; Zhong, L.; Liu, H.; Fang, Z.; Yan, C.; Chen, M.; Kong, Y.; Lee, C.; Liu, D.; Li, S.; Liu, J.; Song, L.; Chen, G.; Yan, Q.; Yu, G. Selective electrocatalytic synthesis of urea with nitrate and carbon dioxide. *Nat. Sustain.* **2021**, *4* (10), 868–876.
- (11) Wu, Y.; Jiang, Z.; Lin, Z.; Liang, Y.; Wang, H. Direct electrosynthesis of methylamine from carbon dioxide and nitrate. *Nat. Sustain.* **2021**, *4* (8), 725–730.
- (12) Chen, C.; Zhu, X.; Wen, X.; Zhou, Y.; Zhou, L.; Li, H.; Tao, L.; Li, Q.; Du, S.; Liu, T.; Yan, D.; Xie, C.; Zou, Y.; Wang, Y.; Chen, R.; Huo, J.; Li, Y.; Cheng, J.; Su, H.; Zhao, X.; Cheng, W.; Liu, Q.; Lin, H.; Luo, J.; Chen, J.; Dong, M.; Cheng, K.; Li, C.; Wang, S. Coupling N<sub>2</sub> and CO<sub>2</sub> in H<sub>2</sub>O to synthesize urea under ambient conditions. *Nat. Chem.* **2020**, *12* (8), 717–724.
- (13) Yuan, M.; Chen, J.; Bai, Y.; Liu, Z.; Zhang, J.; Zhao, T.; Wang, Q.; Li, S.; He, H.; Zhang, G. Unveiling electrochemical urea synthesis by co-activation of CO<sub>2</sub> and N<sub>2</sub> with mott-schottky heterostructure catalysts. *Angew. Chem., Int. Ed. Engl.* **2021**, *60* (19), 10910–10918.
- (14) Mukherjee, J.; Paul, S.; Adalder, A.; Kapse, S.; Thapa, R.; Mandal, S.; Ghorai, B.; Sarkar, S.; Ghorai, U. K. Understanding the site-selective electrocatalytic co-reduction mechanism for green urea synthesis using copper phthalocyanine nanotubes. *Adv. Funct. Mater.* **2022**, 2200882.
- (15) Leverett, J.; Tran-Phu, T.; Yuwono, J. A.; Kumar, P.; Kim, C.; Zhai, Q.; Han, C.; Qu, J.; Cairney, J.; Simonov, A. N.; Hocking, R. K.; Dai, L.; Daiyan, R.; Amal, R. Tuning the coordination structure of Cu-N-C single atom catalysts for simultaneous electrochemical reduction of CO<sub>2</sub> and NO<sub>3</sub><sup>-</sup> to urea. *Adv. Energy Mater.* **2022**, 2201500.
- (16) Huang, Y.; Yang, R.; Wang, C.; Meng, N.; Shi, Y.; Yu, Y.; Zhang, B. Direct electrosynthesis of urea from carbon dioxide and nitric oxide. *ACS Energy Letters* **2022**, *7*, 284–291.
- (17) Feng, Y.; Yang, H.; Zhang, Y.; Huang, X.; Li, L.; Cheng, T.; Shao, Q. Te-doped Pd nanocrystal for electrochemical urea production by efficiently coupling carbon dioxide reduction with nitrite reduction. *Nano Lett.* **2020**, *20* (11), 8282–8289.
- (18) Rooney, C. L.; Wu, Y.; Tao, Z.; Wang, H. Electrochemical reductive N-methylation with CO<sub>2</sub> enabled by a molecular catalyst. *J. Am. Chem. Soc.* **2021**, *143* (47), 19983–19991.
- (19) Li, Y.; Zheng, S.; Liu, H.; Xiong, Q.; Yi, H.; Yang, H.; Mei, Z.; Zhao, Q.; Yin, Z. W.; Huang, M.; Lin, Y.; Lai, W.; Dou, S. X.; Pan, F.; Li, S. Sequential co-reduction of nitrate and carbon dioxide enables selective urea electrosynthesis. *Nat. Commun.* **2024**, *15* (1), 176.
- (20) Li, L.; Tang, C.; Jin, H.; Davey, K.; Qiao, S.-Z. Main-group elements boost electrochemical nitrogen fixation. *Chem.* **2021**, *7* (12), 3232–3255.
- (21) McIsaac, G. F.; David, M. B.; Gertner, G. Z.; Goolsby, D. A. Nitrate flux in the mississippi river. *Nature* **2001**, *414* (6865), 710–710.
- (22) Wang, Z.; Richards, D.; Singh, N. Recent discoveries in the reaction mechanism of heterogeneous electrocatalytic nitrate reduction. *Catalysis Science & Technology* **2021**, *11* (3), 705–725.
- (23) Zheng, S.; Liang, X.; Pan, J.; Hu, K.; Li, S.; Pan, F. Multi-center cooperativity enables facile C–C coupling in electrochemical CO<sub>2</sub> reduction on a Ni<sub>2</sub>P catalyst. *ACS Catal.* **2023**, *13* (5), 2847–2856.
- (24) Bagger, A.; Arnarson, L.; Hansen, M. H.; Spohr, E.; Rossmelil, J. Electrochemical CO reduction: A property of the electrochemical interface. *J. Am. Chem. Soc.* **2019**, *141* (4), 1506–1514.
- (25) Bai, X.; Zhao, X.; Zhang, Y.; Ling, C.; Zhou, Y.; Wang, J.; Liu, Y. Dynamic stability of copper single-atom catalysts under working conditions. *J. Am. Chem. Soc.* **2022**, *144* (37), 17140–17148.
- (26) Liu, X.; Jiao, Y.; Zheng, Y.; Jaroniec, M.; Qiao, S. Z. Mechanism of C-N bonds formation in electrocatalytic urea production revealed by ab initio molecular dynamics simulation. *Nat. Commun.* **2022**, *13* (1), 5471.
- (27) Ding, H.; Zheng, S.; Yang, X.; Pan, J.; Chen, Z.; Zhang, M.; Li, S.; Pan, F. Role of surface hydrogen coverage in C–C coupling process for CO<sub>2</sub> electroreduction on Ni-based catalysts. *ACS Catal.* **2024**, *14* (19), 14330–14338.
- (28) Zheng, S.; Zuo, C.; Liang, X.; Li, S.; Pan, F. Valence state of transition metal center as an activity descriptor for CO<sub>2</sub> reduction on single atom catalysts. *Journal of Energy Chemistry* **2021**, *56*, 444–448.
- (29) Zhao, Q.; Xu, Y.; Greeley, J.; Savoie, B. M. Deep reaction network exploration at a heterogeneous catalytic interface. *Nat. Commun.* **2022**, *13* (1), 4860.
- (30) Ulissi, Z. W.; Medford, A. J.; Bligaard, T.; Nørskov, J. K. To address surface reaction network complexity using scaling relations machine learning and DFT calculations. *Nat. Commun.* **2017**, *8*, 14621.

- (31) Zhao, Q.; Savoie, B. M. Simultaneously improving reaction coverage and computational cost in automated reaction prediction tasks. *Nature Computational Science* **2021**, *1* (7), 479–490.
- (32) Liu, J. C.; Ma, X. L.; Li, Y.; Wang, Y. G.; Xiao, H.; Li, J. Heterogeneous Fe<sub>3</sub> single-cluster catalyst for ammonia synthesis via an associative mechanism. *Nat. Commun.* **2018**, *9* (1), 1610.
- (33) Bajdich, M.; Garcia-Mota, M.; Vojvodic, A.; Norskov, J. K.; Bell, A. T. Theoretical investigation of the activity of cobalt oxides for the electrochemical oxidation of water. *J. Am. Chem. Soc.* **2013**, *135* (36), 13521–30.
- (34) Cheng, T.; Xiao, H.; Goddard, W. A., 3rd Full atomistic reaction mechanism with kinetics for CO reduction on Cu(100) from ab initio molecular dynamics free-energy calculations at 298 K. *Proc. Natl. Acad. Sci. U. S. A.* **2017**, *114* (8), 1795–1800.
- (35) Qin, X.; Vegge, T.; Hansen, H. A. Cation-coordinated inner-sphere CO<sub>2</sub> electroreduction at Au–water interfaces. *J. Am. Chem. Soc.* **2023**, *145* (3), 1897–1905.
- (36) Cheng, T.; Xiao, H.; Goddard, W. A., 3rd Reaction mechanisms for the electrochemical reduction of CO<sub>2</sub> to CO and formate on the Cu(100) surface at 298 K from quantum mechanics free energy calculations with explicit water. *J. Am. Chem. Soc.* **2016**, *138* (42), 13802–13805.
- (37) Gu, G. H.; Lee, M.; Jung, Y.; Vlachos, D. G. Automated exploitation of the big configuration space of large adsorbates on transition metals reveals chemistry feasibility. *Nat. Commun.* **2022**, *13* (1), 2087.
- (38) Boes, J. R.; Mamun, O.; Winther, K.; Bligaard, T. Graph theory approach to high-throughput surface adsorption structure generation. *J. Phys. Chem. A* **2019**, *123* (11), 2281–2285.
- (39) Gu, T.; Wang, B.; Chen, S.; Yang, B. Automated generation and analysis of the complex catalytic reaction network of ethanol synthesis from syngas on Rh(111). *ACS Catal.* **2020**, *10* (11), 6346–6355.
- (40) Su, X.; Yang, X. F.; Huang, Y.; Liu, B.; Zhang, T. Single-atom catalysis toward efficient CO<sub>2</sub> conversion to CO and formate products. *Acc. Chem. Res.* **2019**, *52* (3), 656–664.
- (41) Zhai, Y.; Zhu, Z.; Zhu, C.; Chen, K.; Zhang, X.; Tang, J.; Chen, J. Single-atom catalysts boost nitrogen electroreduction reaction. *Mater. Today* **2020**, *38*, 99–113.
- (42) Cheng, Y.; Yang, S.; Jiang, S. P.; Wang, S. Supported single atoms as new class of catalysts for electrochemical reduction of carbon dioxide. *Small Methods* **2019**, 1800440.
- (43) Peng, Y.; Lu, B.; Chen, S. Carbon-supported single atom catalysts for electrochemical energy conversion and storage. *Adv. Mater.* **2018**, *30* (48), No. e1801995.
- (44) Lovrić, M.; Molero, J. M.; Kern, R. PySpark and RDKit: moving towards big data in cheminformatics. *Mol. Inform.* **2019**, *38* (6), No. e1800082.
- (45) Weng, M.; Wang, Z.; Qian, G.; Ye, Y.; Chen, Z.; Chen, X.; Zheng, S.; Pan, F. Identify crystal structures by a new paradigm based on graph theory for building materials big data. *Science China Chemistry* **2019**, *62* (8), 982–986.
- (46) Li, S.; Chen, Z.; Wang, Z.; Weng, M.; Li, J.; Zhang, M.; Lu, J.; Xu, K.; Pan, F. Graph-based discovery and analysis of atomic-scale one-dimensional materials. *Natl. Sci. Rev.* **2022**, *9* (6), 28.
- (47) Liu, T.; Wang, Y.; Li, Y. Can Metal-nitrogen-carbon single-atom catalysts boost the electroreduction of carbon monoxide? *JACS Au* **2023**, *3* (3), 943–952.
- (48) Tang, C.; Chen, L.; Li, H.; Li, L.; Jiao, Y.; Zheng, Y.; Xu, H.; Davey, K.; Qiao, S. Z. Tailoring acidic oxygen reduction selectivity on single-atom catalysts via modification of first and second coordination spheres. *J. Am. Chem. Soc.* **2021**, *143* (20), 7819–7827.
- (49) Guo, H.; Zhu, H.; Liu, G.-Y.; Chen, Z.-X. General reaction network exploration scheme based on graph theory representation and depth first search applied to CO<sub>2</sub> hydrogenation on Pd<sub>2</sub>Cu catalyst. *ACS Catal.* **2024**, *14* (8), 5720–5734.
- (50) Hashemi, A.; Bougueroua, S.; Gageot, M. P.; Pidko, E. A. ReNeGate: A reaction network graph-theoretical tool for automated mechanistic studies in computational homogeneous catalysis. *J. Chem. Theory Comput.* **2022**, *18* (12), 7470–7482.
- (51) Dijkstra, E. W. A note on two problems in connexion with graphs. *Edsger Wybe Dijkstra: His Life, Work, and Legacy* **2022**, 287–290.
- (52) Xu, M.; Wu, F.; Zhang, Y.; Yao, Y.; Zhu, G.; Li, X.; Chen, L.; Jia, G.; Wu, X.; Huang, Y.; Gao, P.; Ye, W. Kinetically matched C–N coupling toward efficient urea electrosynthesis enabled on copper single-atom alloy. *Nat. Commun.* **2023**, *14* (1), 6994.
- (53) Zhou, Y.; Yang, B.; Huang, Z.; Chen, G.; Tang, J.; Liu, M.; Liu, X.; Ma, R.; Mei, Z.; Zhang, N. Cu–Ni alloy nanocrystals with heterogeneous active sites for efficient urea synthesis. *Applied Catalysis B: Environmental* **2024**, *343*, No. 123577.
- (54) Gao, Y.; Wang, J.; Sun, M.; Jing, Y.; Chen, L.; Liang, Z.; Yang, Y.; Zhang, C.; Yao, J.; Wang, X. Tandem catalysts enabling efficient C–N coupling toward the electrosynthesis of urea. *Angew. Chem., Int. Ed. Engl.* **2024**, *63* (23), No. e202402215.
- (55) Zhong, Y.; Xiong, H.; Low, J.; Long, R.; Xiong, Y. Recent progress in electrochemical C–N coupling reactions. *eScience* **2023**, *3* (1), 100086.
- (56) Zheng, S.; Li, S.; Mei, Z.; Hu, Z.; Chu, M.; Liu, J.; Chen, X.; Pan, F. Electrochemical nitrogen reduction reaction performance of single-boron catalysts tuned by MXene substrates. *J. Phys. Chem. Lett.* **2019**, *10* (22), 6984–6989.
- (57) Ling, C.; Ouyang, Y.; Li, Q.; Bai, X.; Mao, X.; Du, A.; Wang, J. A general two-step strategy–based high-throughput screening of single atom catalysts for nitrogen fixation. *Small Methods* **2018**, 1800376.
- (58) Hai, X.; Xi, S.; Mitchell, S.; Harrath, K.; Xu, H.; Akl, D. F.; Kong, D.; Li, J.; Li, Z.; Sun, T.; Yang, H.; Cui, Y.; Su, C.; Zhao, X.; Li, J.; Perez-Ramirez, J.; Lu, J. Scalable two-step annealing method for preparing ultra-high-density single-atom catalyst libraries. *Nat. Nanotechnol.* **2022**, *17* (2), 174–181.
- (59) Lai, W. H.; Wang, H.; Zheng, L.; Jiang, Q.; Yan, Z. C.; Wang, L.; Yoshikawa, H.; Matsumura, D.; Sun, Q.; Wang, Y. X.; Gu, Q.; Wang, J. Z.; Liu, H. K.; Chou, S. L.; Dou, S. X. General synthesis of single-atom catalysts for hydrogen evolution reactions and room-temperature Na–S batteries. *Angew. Chem., Int. Ed. Engl.* **2020**, *59* (49), 22171–22178.
- (60) Liu, S.; Li, Z.; Wang, C.; Tao, W.; Huang, M.; Zuo, M.; Yang, Y.; Yang, K.; Zhang, L.; Chen, S.; Xu, P.; Chen, Q. Turning main-group element magnesium into a highly active electrocatalyst for oxygen reduction reaction. *Nat. Commun.* **2020**, *11* (1), 938.
- (61) Jiang, Z.; Wang, T.; Pei, J.; Shang, H.; Zhou, D.; Li, H.; Dong, J.; Wang, Y.; Cao, R.; Zhuang, Z.; Chen, W.; Wang, D.; Zhang, J.; Li, Y. Discovery of main group single Sb–N<sub>4</sub> active sites for CO<sub>2</sub> electroreduction to formate with high efficiency. *Energy Environ. Sci.* **2020**, *13* (9), 2856–2863.
- (62) Zhang, D.; Bi, H.; Dai, F. Z.; Jiang, W.; Liu, X.; Zhang, L.; Wang, H. Pretraining of attention-based deep learning potential model for molecular simulation. *npj Comput. Mater.* **2024**, *10* (1), 94.
- (63) Lan, J.; Palizhati, A.; Shuaibi, M.; Wood, B. M.; Wander, B.; Das, A.; Uyttendaele, M.; Zitnick, C. L.; Ulissi, Z. W. AdsorbML: a leap in efficiency for adsorption energy calculations using generalizable machine learning potentials. *npj Comput. Mater.* **2023**, *9* (1), 172.
- (64) Shi, Y. F.; Kang, P. L.; Shang, C.; Liu, Z. P. Methanol Synthesis from CO<sub>2</sub>/CO Mixture on Cu–Zn catalysts from microkinetics-guided machine learning pathway search. *J. Am. Chem. Soc.* **2022**, *144* (29), 13401–13414.
- (65) Zheng, S.; Yang, X.; Shi, Z. Z.; Ding, H.; Pan, F.; Li, J. F. The loss of interfacial water-adsorbate hydrogen bond connectivity position surface-active hydrogen as a crucial intermediate to enhance nitrate reduction reaction. *J. Am. Chem. Soc.* **2024**, *146* (39), 26965–26974.
- (66) Yang, X.; Ding, H.; Li, S.; Zheng, S.; Li, J.-F.; Pan, F. Cation-induced interfacial hydrophobic microenvironment promotes the C–C coupling in electrochemical CO<sub>2</sub> reduction. *J. Am. Chem. Soc.* **2024**, *146* (8), 5532–5542.
- (67) Wang, Y.-H.; Zheng, S.; Yang, W.-M.; Zhou, R.-Y.; He, Q.-F.; Radjenovic, P.; Dong, J.-C.; Li, S.; Zheng, J.; Yang, Z.-L.; Attard, G.;

Pan, F.; Tian, Z.-Q.; Li, J.-F. In situ Raman spectroscopy reveals the structure and dissociation of interfacial water. *Nature* **2021**, *600* (7887), 81–85.

(68) Peterson, A. A.; Abild-Pedersen, F.; Studt, F.; Rossmeisl, J.; Nørskov, J. K. How copper catalyzes the electroreduction of carbon dioxide into hydrocarbon fuels. *Energy Environ. Sci.* **2010**, *3* (9), 1311.

(69) Hu, X.; Chen, S.; Chen, L.; Tian, Y.; Yao, S.; Lu, Z.; Zhang, X.; Zhou, Z. What is the real origin of the activity of Fe-N-C electrocatalysts in the O<sub>2</sub> reduction reaction? critical roles of coordinating pyrrolic N and axially adsorbing species. *J. Am. Chem. Soc.* **2022**, *144* (39), 18144–18152.

(70) Kresse, G.; Hafner, J. Ab initio molecular dynamics for liquid metals. *Phys. Rev. B* **1993**, *47* (1), 558.

(71) Kresse, G.; Furthmüller, J. Efficiency of ab-initio total energy calculations for metals and semiconductors using a plane-wave basis set. *Comput. Mater. Sci.* **1996**, *6* (1), 15–50.

(72) Kresse, G.; Furthmüller, J. Efficient iterative schemes for ab initio total-energy calculations using a plane-wave basis set. *Phys. Rev. B* **1996**, *54* (16), 11169.

(73) Perdew, J. P.; Burke, K.; Ernzerhof, M. Generalized gradient approximation made simple. *Physical review letters* **1996**, *77* (18), 3865.

(74) Kresse, G.; Joubert, D. From ultrasoft pseudopotentials to the projector augmented-wave method. *Phys. Rev. B* **1999**, *59* (3), 1758.

(75) Blöchl, P. E. Projector augmented-wave method. *Phys. Rev. B* **1994**, *50* (24), 17953.

(76) Mathew, K.; Kolluru, V. S. C.; Mula, S.; Steinmann, S. N.; Hennig, R. G. Implicit self-consistent electrolyte model in plane-wave density-functional theory. *J. Chem. Phys.* **2019**, *151* (23), 234101.

(77) Lovrić, M.; Molero, J. M.; Kern, R. PySpark and RDKit: moving towards big data in cheminformatics. *Mol. Informatics* **2019**, *38* (6), 1800082.



CAS BIOFINDER DISCOVERY PLATFORM™

## BRIDGE BIOLOGY AND CHEMISTRY FOR FASTER ANSWERS

Analyze target relationships,  
compound effects, and disease  
pathways

Explore the platform

